ORIGINAL ARTICLE

lajss.org
Latin American Journal of Solids and Structures

www.lajss.org

Influence of stress triaxiality on the fracture behaviour of Ti6Al4V alloy manufactured by electron beam melting

Tiago Sartor[a], Jorge Vicente Lopes da Silva[b], Zhongwei Guan[c], Rafael Celeghini Santiago[d,e*]

[a]Centro de Engenharia e Ciências Sociais Aplicadas (CECS), Universidade Federal do ABC (UFABC), São Bernardo do Campo, SP, Brasil. E-mails: tiago_sartor@hotmail.com
[b]Centro de Tecnologia da Informação Renato Archer (CTI), Campinas, SP, Brasil. E-mail: jorge.silva@cti.gov.br
[c]Advanced Materials Research Centre, Technology Innovation Institute, Abu Dhabi, United Arab Emirates. E-mail: zhongwei.guan@tii.ae
[d]Centro de Engenharia e Ciências Sociais Aplicadas (CECS), Universidade Federal do ABC (UFABC), São Bernardo do Campo, SP, Brasil. E-mails: rafael.santiago@ufabc.edu.br
[e]Advanced Materials Research Centre, Technology Innovation Institute, Abu Dhabi, United Arab Emirates. E-mail: rafael.santiago@tii.ae

* Corresponding author.

https://doi.org/10.1590/1679-78257293

Abstract

This paper aims to investigate the influence of stress triaxiality on the fracture behaviour of Ti6Al4V fabricated by Electron Beam Melting (EBM). Here, specimens with seven configurations were manufactured and tested to obtain a wide range of stress triaxialities. A combined approach using Digital Image Correlation (DIC) and finite element (FE) modelling was used to evaluate the current stress triaxiality levels of the various specimens. The material fracture envelope was defined with the triaxiality in a range from -0.28 to 0.71, noting that the fracture was strongly dependent on the stress triaxiality. The characterisations were then carried out by testing an ad-hoc specimen to evaluate failure criteria at low and high stress triaxialities. It was shown that the FE model using the failure criterion based on triaxiality offers more accurate predictions of the material's failure response than that based on the effective plastic strain. The modelling approach based on anisotropic elasto-plasticity contributes to better predictions of the alloy's response. Thus, the failure models based on the stress triaxiality are highly recommended for producing accurate numerical predictions of the fracture response of Ti6Al4V-EBM.

Keywords

Stress triaxiality, fracture, additive manufacturing, electron beam melting, Ti6Al4V.

Graphical Abstract

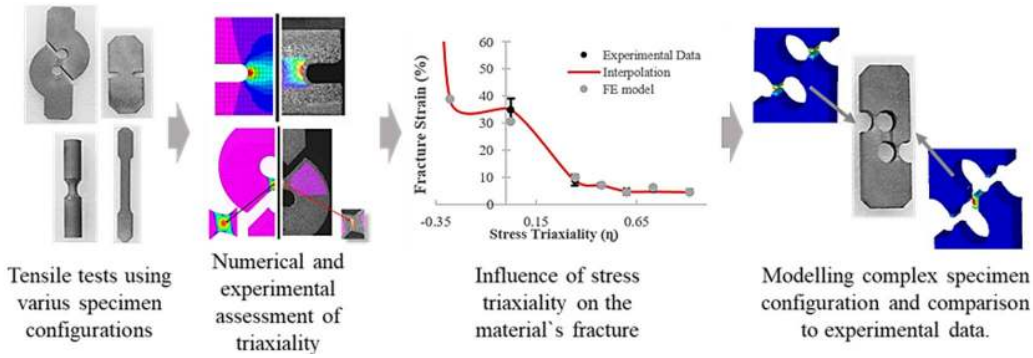

Received: September 12, 2022. In revised form: October 18, 2022. Accepted: October 21, 2022. Available online: November 01, 2022.
https://doi.org/10.1590/1679-78257293

Latin American Journal of Solids and Structures. ISSN 1679-7825. Copyright © 2022. This is an Open Access article distributed under the terms of the Creative Commons Attribution License, which permits unrestricted use, distribution, and reproduction in any medium, provided the original work is properly cited.

1 INTRODUCTION

Additive manufacturing (AM) technologies have enabled the fabrication of optimised complex structures that are otherwise unattainable with simplifying machinery and reducing structural weight, development cost and time. In particular, the Powder Bed Fusion technologies [1], such as Electron Beam Melting (EBM), are currently used to manufacture complex metallic components from a wide range of alloys, such as stainless steel, aluminium and titanium [2]. Thus, EBM has broadened AM's applications, as it allows manufacturing dense metallic components that can be used as primary structural components. Beyond the aerospace sector, EBM has been deployed to manufacture high-quality devices for medical and dental applications, in which titanium alloy Ti6Al4V has been commonly used due to its superior mechanical strength and biocompatibility [3-5]. However, EBM results in material properties highly dependent on the manufacturing parameters, such as beam energy, scanning velocities and melting strategy [6-9].

A comprehensive understanding of the material's mechanical response under elastic, plastic and failure regimes is needed for modelling the structural response when subjected to ultimate limit state conditions. Commercial numerical software with advanced element formulation and failure criteria have been proven to have the capability of predicting the structural response of materials and structures, with a reduced number of experimental evaluations for design or assessment purposes [10-15, 17-18]. Commonly used failure criteria, such as effective-plastic strain (EPS), maximum shear strain or von Mises have limitations for predicting the mechanical response of ductile materials when subjected to different types of loadings, e.g. combined tension and shear-dominated loading conditions. Usually, those criteria are suitable for a narrow range of applications [10].

Bao [11] and Wierzbicki et al. [12] identified a single failure criterion that could be suitable for a wide range of applications, such as compression, tension and shear. Wierzbicki et al. [12] pointed out that stress triaxiality, η, could quantify the stress distribution and then the failure condition for ductile materials. Furthermore, the triaxiality-based failure criterion was able to count for the influence of distinctive fracture mechanisms, such as shear-dominated, stretch-dominated and mixed ones. Ductile failure modes, governed by void nucleation, growth and coalescence, are expected for $\eta>1/3$; meanwhile, shear-dominated failures at $-1/3<\eta<0$ and mixed-mode for $0<\eta<1/3$, are also shown a lower limit for fracture of ductile materials as $\eta=-1/3$ [13].

Wierzbicki et al. [12] explored the influence of stress triaxiality on fracture in 2024-T351 aluminium alloy by using several failure models with seven specimen configurations subjected to various triaxiality levels. They proposed the Xue-Wierzbicki fracture criterion that presented a good performance for predicting the failure at different triaxiality levels for a given alloy. Wenchao et al. [14] evaluated the effects of stress triaxiality and Lode angle on the fracture mechanism of the high-strength steel alloy Q460 using four specimens types. It was noted that the material exhibited the response expected for ductile materials, changing from shear-dominated to stretch-dominated fracture modes as stress triaxiality increases. The finite element (FE) models were also used for evaluating the current stress triaxiality state at the onset of material failure. A similar procedure for studying the influence of triaxiality was also performed by Calle et al. [15] for predicting the fracture behaviour of low-carbon shipbuilding steel alloy, which was complemented by digital image correlation (DIC) to measure the localised strain field. Sjöberg et al. [16] explored the nickel alloy 718 at the stress triaxialities in a range from 0.05 to 0.50 using four different specimen configurations, highlighting the material fracture dependence on the stress state.

To assess different ductile failure criteria, Dreamier et al. [10] proposed an ad-hoc specimen to generate distinct failure modes at low and high triaxiality in one single tensile test, so-called bifailure. Those failures occur at high- and low-stress triaxiality levels, such as tension- and shear-dominated, respectively, which can also be tailored. This work also explored the performance of different failure criteria applicable for predicting material failure behaviour at different stress triaxiality levels, noting that failure criteria that define an abrupt failure limit, such as EPS. Vigano et al. [17] and Morales et al. [18] evaluated different failure criteria for predicting the fracture of automotive bumpers, highlighting the advantages of Johnson-Cook damage criteria compared to the maximum shear stress and EPS failure criteria.

Tang et al. [19] and Hammer et al. [20] studied the fracture mechanics of Ti6Al4V specimens made by casting and cold-rolling. The studies investigated the fracture response of the specimens under different uniaxial, bi-axial and shear loading conditions to identify the forming limit curve suitable for the material. It was noted that the alloy presented an anisotropic ductile failure behaviour according to the lamination direction and through-thickness direction. The influence of stress triaxiality on Ti6Al4V parts was also pointed out by Mocko et al. [21] and Wang et al. [22]. Hammer et al. [20] performed characterisations of the same alloy under the plastic regime and fracture at different strain rates, temperatures and stress triaxialities. Those parameters were used to develop numerical models using the commercial code LS-Dyna, which demonstrated an accurate prediction of the material's response. The numerical modelling of the fracture behaviour of Ti6Al4V alloy was also developed by Ziaja et al. [23]

To the best of the authors' knowledge, only limited studies investigate the fracture mechanisms of Ti6Al4V parts made by EBM [9]. Zhai et al. [24] compared the microstructure, tensile properties, and damage mechanisms of the alloy processed by EBM and Laser Engineered Net Shaping (LENS). It was noted that EBM yielded alloys with a unique microstructure comprising α+β lamellae, with superior yield and ultimate strengths, and the interaction between those phases governed the fracture mechanisms. The ductile damage behaviour of BEM Ti6Al4V was also studied by Nalli et al. [25]. However, no other references were found in the public domain in quantifying the effect of stress triaxiality on the material fracture.

Therefore, this paper aims to explore the influence of stress triaxiality on the fracture behaviour of Ti6Al4V parts made by EBM. Here, specimens with various configurations were manufactured and evaluated by microscopy, surface roughness and hardness. The elasto-plastic response of the material was obtained by using a universal testing machine, which was further numerically modelled. Then, the material fracture behaviour was explored by numerical and experimental approaches, with the influence of stress triaxiality on the material fracture strain. Finally, the FE model was developed to simulate the mechanical response of an ad-hoc sample with complex configurations, compared to experimental measurements with 3D DIC to validate the methodology used.

2 MATERIALS AND METHODS

The methodology used to conduct this work is summarised in Figure 1. Seven specimen configurations were chosen to capture the elasto-plastic behaviour and the fracture strain at various triaxiality levels. Once the specimen configurations were defined, the samples were then manufactured by EBM, with its roughness, hardness, porosity and microstructure being characterised. The elasto-plastic response of the material was obtained by a series of tensile and compressive tests. The samples were numerically modelled and compared to experimental results, aiming at an accurate definition of the stress triaxiality level corresponding to fracture. Finally, the fracture parameters were defined and obtained by testing an ad-hoc double fracture specimen called `bifailure` [10]. This specimen was also manufactured by EBM, with its performance being numerically modelled. The results from both the test and numerical modelling were compared to provide the necessary validation.

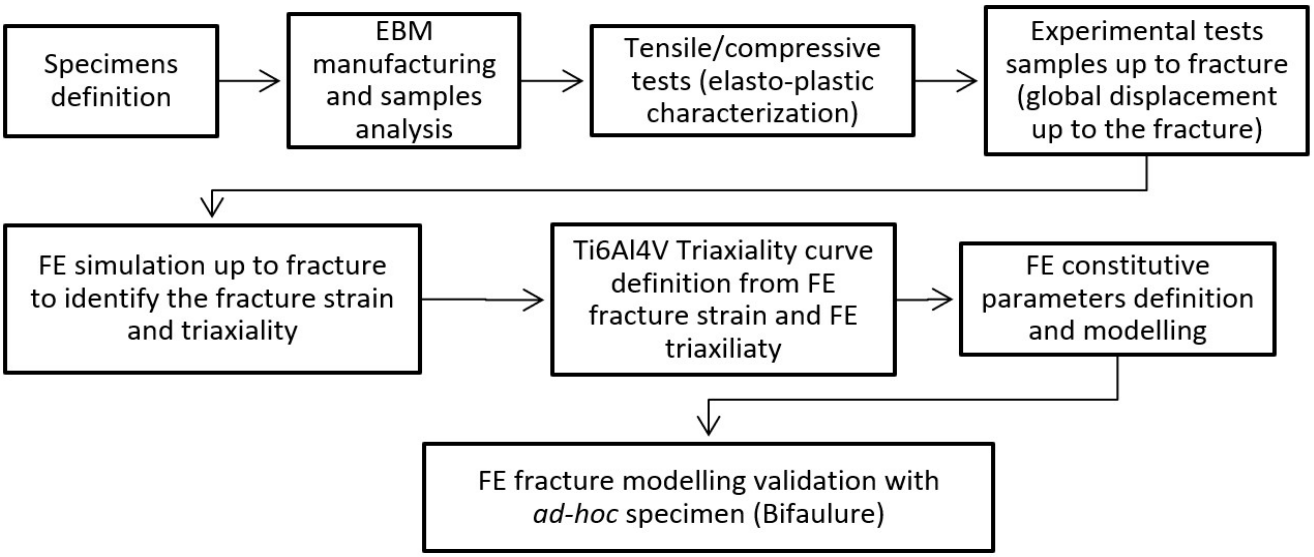

Figure 1: Workflow followed for the mechanical characterisation of Ti6Al4V made by EBM under elastic, plastic and failure regimes.

All samples were manufactured by EBM technique in Arcam Q10 machine, using Ti6Al4V powder [27], with the nominal composition being shown in Table 1, deploying the manufacturing parameters being listed in Table 2. The feedstock used was a fresh powder and all the samples were manufactured simultaneously. No surface finishing, post-processing and heat-treatment were carried out on the samples produced, with the support material being extracted by localised grinding to separate parts from the base plate. The chemical compositions of the samples were evaluated by Energy Dispersive x-ray Spectroscopy (EDS) (ThermoFisher Scientific, model K-Alpha+). As EDS is a quasi-qualitative technique [26], there is a slight reduction of the aluminum composition, and a vanadium excess in the alloy is measured. EDS did not identify other remaining compositions due to the small amounts presented.

Table 1: Chemical composition of Ti-6Al-4V alloy Grade 5 used.

Ti-6Al-4V (Grade 5) Arcam EBM System: chemical composition (w. %)								
	Al	**V**	**C**	**Fe**	**O**	**N**	**H**	**Ti**
Powder [26]	6.00 ± 0.25	4.00 ± 0.50	0.03	0.10	0.10	0.01	< 0.003	Balance
Manufactured samples	5.18 ± 0.16	5.62 ± 0.81	-	-	-	-	-	Balance

Table 2: Manufacturing specifications.

Material	**Ti6Al4V Grade 5**
Particle size	Between 45 and 106 µm
Potential difference	60 kV
Current	41 mA
Beam power	2460 W
Layer thickness	52 µm
Base plate temperature	360 ºC
Scanning velocity	4.53 m/s
Energy density	543 J/m

All the samples were manufactured with their long axis perpendicular to the build plate (z-direction), i.e. with the loading direction parallel to the build direction [28], according to Figure 2(a). In order to study different levels of stress triaxiality, specimens with seven configurations were proposed to cover a triaxiality range from -0.28 to 0.90. An additional bifailure specimen configuration was also used for evaluating the performance of the numerical model. Figure 2(b) shows the specimen configurations after manufacturing.

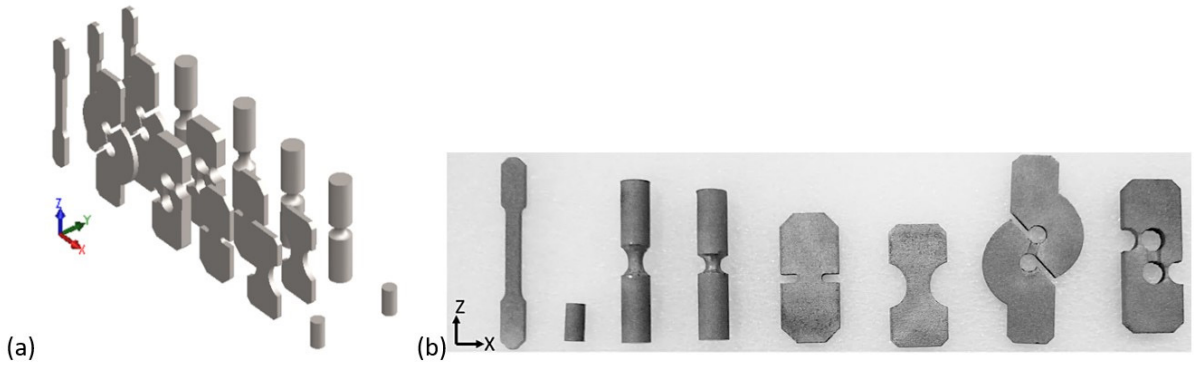

Figure 2: (a) Specimen distribution within the build chamber and (b) specimen configurations used.

2.1 Manufacturing quality assessment

The average roughness (Ra) of all printed specimens was measured using a Taylor Hobson Surtronic 3 gauge, with a measuring path of 2.5 mm taken at the x-z, y-z and x-y faces of the specimen (Fig. 2). An optical microscope Zeiss Axio Z1m, with images processed by Axio Vision software, was used to evaluate the resulting porosity. The samples were cut in the x-y plane and polished prior to imaging, following the protocol used in [29]. The same microscope was used to evaluate the resulting microstructure, with the samples being cross-sectioned and polished to a mirror finish for metallographic investigations. The polished cross-sections were chemically etched using a solution of 1.5 v.% hydrofluoric acid (HF), 3.5 v.% nitric acid (HNO3), and distilled water to reveal the grain structure, as proposed by Severino et al. [30]. The material Vickers hardness was measured by a Wilson 420 MVD tester, with10 measurements taken on the x-y and y-z planes.

2.2 Mechanical characterisation

A series of tensile tests were performed in a universal testing machine (Instron 3369) to investigate the elasto-plastic response of Ti6Al4V samples based on ASTM A370-08 [31], Figure 3(a). Therefore, this specimen geometry is

referred to 'St-#', where # is a specimen identification number. The tensile tests were monitored by DIC, using Correlated Solutions VIC-3D software, which allows the full-field measurements of strains in the gauge length up to the ultimate limit state. For this purpose, the samples were painted by a white coating with a random black speckle. The system uses two 5.0 megapixels cameras at a rate of 1 fps, Figure 3(b), with the sample being loaded at a displacement rate of 1 mm/min.

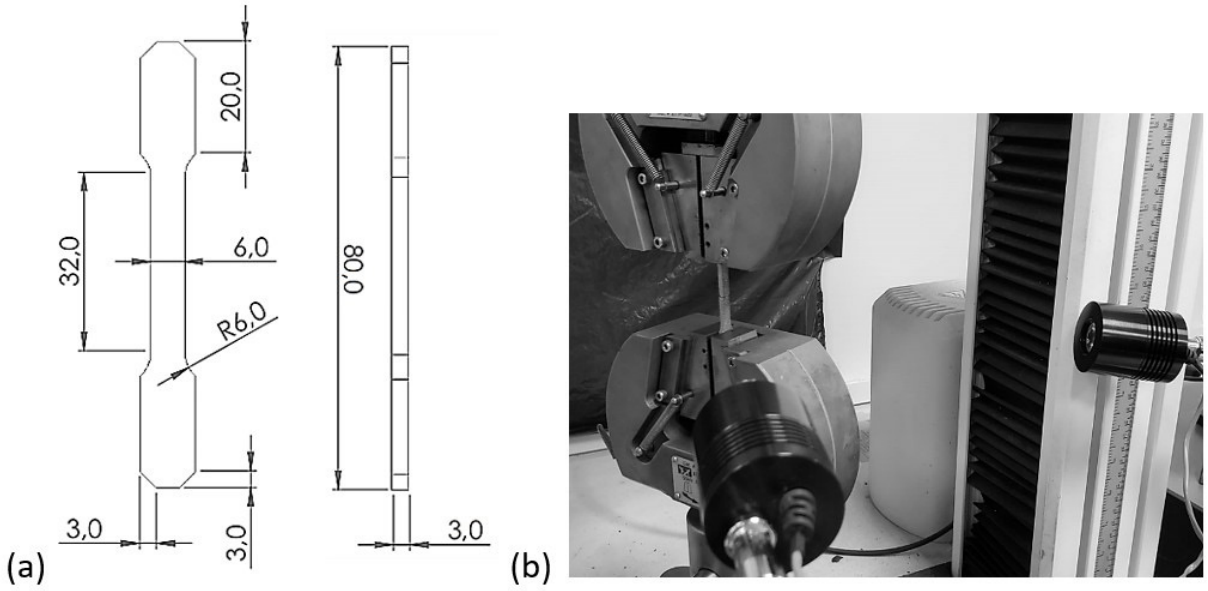

Figure 3 (a) Details of tensile specimen used and (b) tensile test monitored by DIC. (All dimensions in mm).

The true stress of the material, σ_t, (Eq. (1)) was defined by the specimen axial force, F, initial specimen cross-section, A0, and the specimen axial strain, ε, obtained from DIC (Lagragian strain). The plastic constitutive parameters of Ti6Al4V were extracted based on stress-strain curves by using bi-linear and Johnson-Cook (JC) constitutive relationships. The bi-linear model, Eq. (2), defines a tangent plastic modulus, E_t; meanwhile, the Johnson-Cook constitutive relationship defines the material's plasticity as an exponential law, given by Eq. (3).

$$\sigma_t = \frac{F(1+\varepsilon)}{A_0} \tag{1}$$

$$\sigma_p = E_t \varepsilon_p \tag{2}$$

$$\sigma_p = A + B\varepsilon_p^n \tag{3}$$

2.3 Mechanical characterisation Triaxiality and failure

The material stress state can be described by the stress triaxiliaty, which quantifies the spatial stress distribution associated with the material deformation up to the fracture strain. The stress triaxiliaty, η, is the ratio between the hydrostatic stress, σ_{av}, and the equivalent Von Mises, σ_{eq}, which is defined as:

$$\eta = \frac{\sigma_{av}}{\sigma_{eq}} = \frac{\frac{\sigma_1+\sigma_2+\sigma_3}{3}}{\sqrt{\frac{(\sigma_1-\sigma_2)^2+(\sigma_2-\sigma_3)^2+(\sigma_3-\sigma_1)^2}{2}}} \tag{4}$$

Where σ_1, σ_2 and σ_3 are the principal stresses. Thus, seven different specimen configurations were proposed to cover a stress triaxiality range from -0.28 to 0.90. Those configurations were defined based on the previous works [11, 12, 14, 15, 21, 31] and modified according to the limitations of manufacturing and testing devices. The configurations used are shown in Figure 2 and detailed in Table 3 . A specimen identification code was used, also presented in Table 3.

Table 3: Summary of specimen identification code and configurations (dimensions in mm). ('#' gives the specimen number).

Specimen ID Code Triaxiality goal	Specimen configuration	Specimen ID code Triaxiality goal	Specimen configuration
Cp-# $\eta = -0.28$ [12]		Fs-# [2] $\eta = 0.50$ [15]	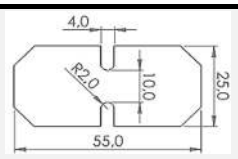
S-# [1] $\eta = -0.09$ [21]	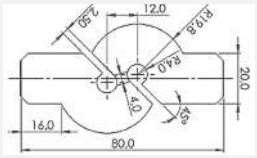	Rb-# $\eta = 0.65$ [14]	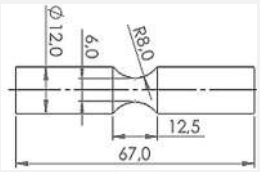
St-# [2,3] $\eta = 0.33$ [31]	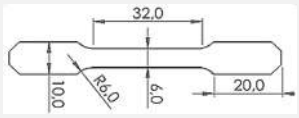	Rs-# $\eta = 0.90$ [11]	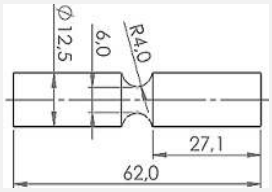
Fb-# [2] $\eta = 0.40$ [15]	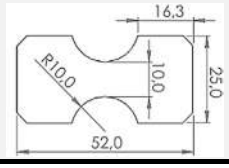		

[1] Thickness at the effective gauge section: 2 mm. [2] Specimen thickness: 3 mm. [3] Based on ASTM A370-08 [31].

Two samples were tested for each configuration in tension using a universal testing machine Instron 3369 at a displacement rate of 1.0 mm/min. The configuration Cp was tested in compression at the same displacement rate. DIC was used to monitor the overall displacement field until the onset of crack formation, except for Cp samples, due to the blocked view by the UTM platens.

The resulting stress triaxialities reached during the test were obtained by modelling the specimens using Altair Optistruct commercial software. The bi-linear material model was used with 0.75 mm hexahedral elements. The specimens were subjected up to the same ultimate global displacement measured by the DIC, and then the stress triaxiality was taken at the place where the failure was initiated. No failure criterion was used in this analysis.

2.4 Fracture modelling and evaluation

The Johnson-Cook (JC) [17] damage parameters were defined and then used to predict the failure of bifailure specimens to evaluate the experimental procedure and methodology used for fracture characterisations of the EBM Ti6Al4V parts. The JC damage model, shown in Eq. (5), has been widely used for modelling the ductile failure of metals, in which the relevant parameters can be defined by representing the influence of stress triaxiality as

$$\varepsilon_f = H_1 + H_2 e^{H_3 \eta} \tag{5}$$

Where ε_f is expressed by the coefficients of H_1, H_2 and H_3, which are defined experimentally. The model assumes that the damage is continuously accumulated at different yielding stages of the material, and the failure occurs when the damage parameter D reaches the critical value of $D_{cr} = 1$, according to

$$D = \begin{cases} 0 \; for \; \sigma_p \leq \sigma_y \\ \int_{\varepsilon_y}^{\varepsilon_p} \frac{1}{\varepsilon_f} d\varepsilon \; for \; \sigma_p > \sigma_y \end{cases} \tag{6}$$

A bifailure specimen, Figure 4(a), was proposed with the radii of the notches selected to reach the triaxiality levels within the range covered in Table 3. This specimen has three critical regions for failure, Figure 4(b), with two at positions 1 and 2, in which the material is subjected at high stress triaxiality level (η>0.3). And another one at position 3, where the material is subjected to low stress triaxiality (0<η<0.05).

The samples were manufactured by EBM and subjected to uniaxial tension in a universal testing machine Instron 3369 at a displacement rate of 1 mm/min and repeated two times. The 3D DIC system was also used to monitor the full-field strain level during the test until the material failure.

The bifailure specimen was modelled using an explicit FE model developed in Ls-Dyna commercial software, Figure 4(c). Here, hexahedral elements with an average size of 0.75 mm were used, which was defined after mesh sensitivity analysis. The JC constitutive parameters with damage were implemented (MAT15: *MAT_JOHNSON_COOK) [32]. The external nodes of the lower specimen part were constrained in all directions, Figure 4(c), meanwhile the external nodes of the upper part were loaded at 1 mm/min in the z-direction. No other boundary constraint was applied. A similar FE model was also developed using the Effective Plastic Strain (EPS) failure criterion for comparison.

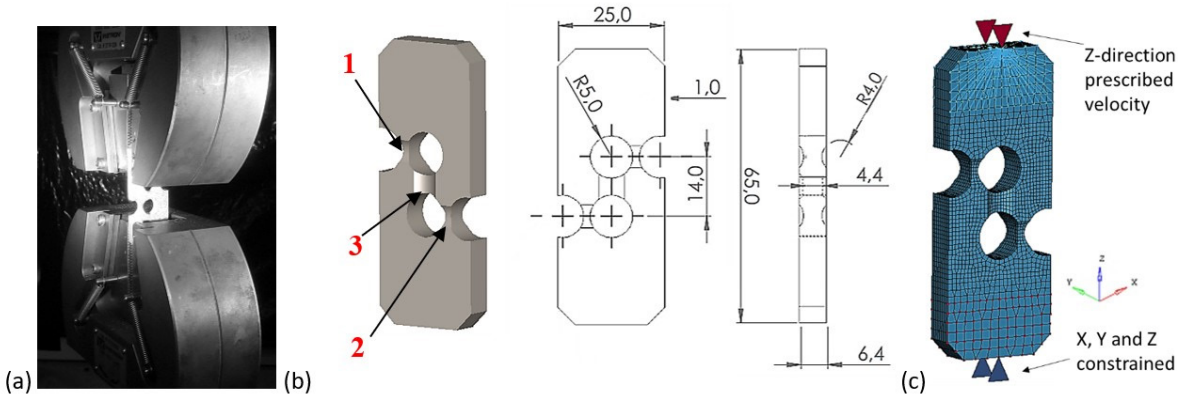

Figure 4: (a) Bifailure specimen used for evaluating damage initiation parameters. (b) Specimen dimensions (in mm).

3 RESULTS AND DISCUSSION

3.1 Surface roughness

Table 4 summarises the roughness (Ra) results. The EBM process resulted in a substantially lower surface roughness, observed on the x-y plane, compared to the x-z and y-z surfaces. Therefore, as expected, the roughness on the sample's upper surface (the x-y plane) was smalled due to the finishing process, which consists of a sequentially melting process with no powder deposition. In another way, the side surfaces (the x-z and y-z planes) exhibit striations dues to the layer deposition. Besides this, it is important to emphasise that the EBM process tends to deliver a higher surface roughness when compared to other AM techniques due to the higher thermal radiation induced by the electron beam and the larger powder size used [5].

Table 4. Surface roughness of Ti6Al-4V samples made by EBM.

Surface plane	x-z	y-z	x-y
Ra (μm)	24.7 ± 1.9	18.0 ± 2.1	4.0 ± 1.3

3.2 Porosity

The material porosity is evident as the black circular spots observed in Figure 5, which seem to be formed by vaporisation or gas entrapment during the melting process, primarily with spherical shapes. According to the image post-processing, it was noted that there was an average porosity of about 2.7 ± 0.2%. Anderson [29] highlighted that this porosity level could significantly influence the fracture mechanism associated with voids nucleation and the stress concentration caused by this, which is also observed in high-stress triaxiality levels.

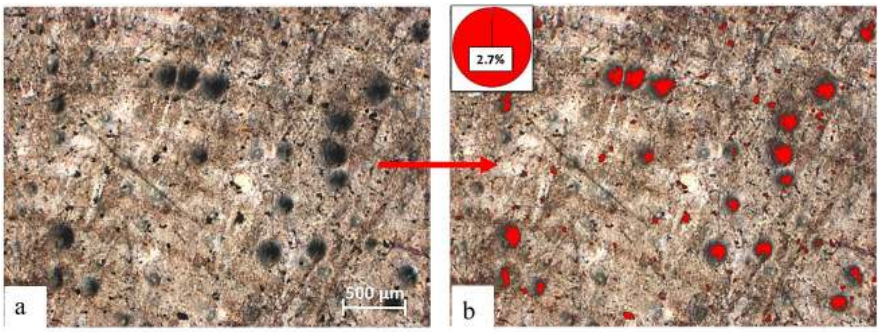

Figure 5: (a) Ti6Al4V samples made by EBM observed by 25x magnification microscope and (b) post-processed by software.

3.3 Hardness

The average hardness was 375.3 ± 11.0 HV and 360.9 ± 7.4 HV on the x-y and y-z planes, respectively. A slight difference was observed between the x-y and the y-z planes, which can indicate an anisotropic behaviour, as reported for this alloy.

3.4 Microstructure

Figure 6 shows the observed microstructure in the x-y and x-z planes. The primary and secondary α-phase lamellae in the original β-phase matrix were observed in both planes, with additional α-precipitation at the grain boundaries at both the x-y and y-z planes. The formation of α colonies in some regions at the x-y plane was also observed.

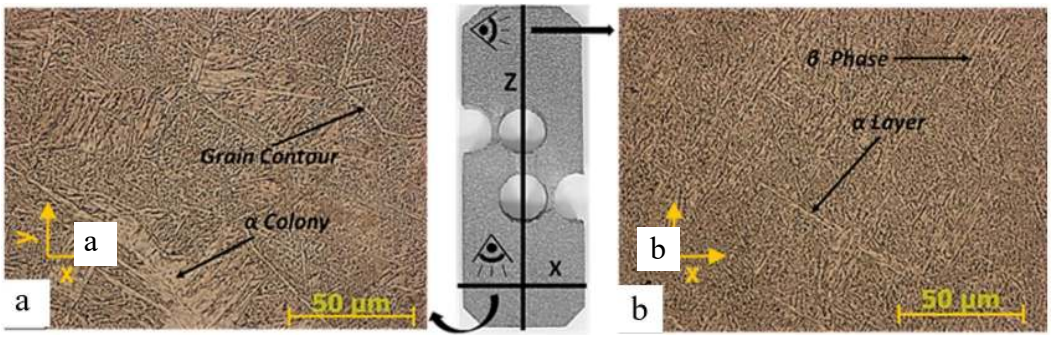

Figure 6: α- and β-phases observed on (a) x-y and (b) y-z-planes of Ti6Al4V samples made by EBM.

3.5 Mechanical characterisation

Figure 7 shows the material strain-stress response that indicates an evident ductile response, with the yield and plastic regions clearly defined. In addition, a reasonably good repeatability was observed between the tested samples. The material plastic constitutive parameters were obtained by curve-fitting, summarised in Table 5.

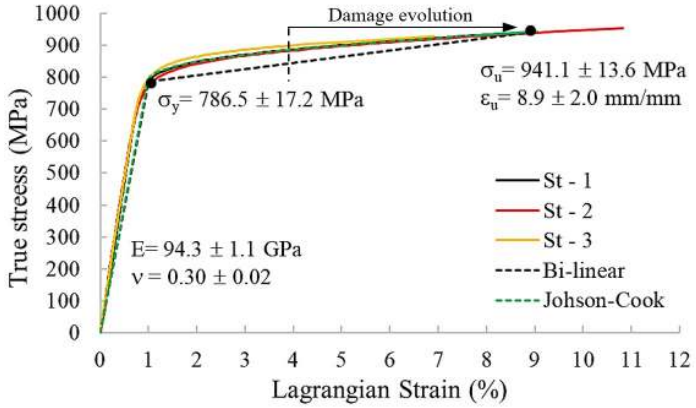

Figure 7: Uniaxial strain-stress curves of the Ti6Al4V alloy made by EBM and its response modelled by bi-linear and Johnson-Cook model, with parameters being elastic modulus, E, Poisson ratio, υ, yield stress, σ_y, ultimate stress, σ_u, and fracture strain, ε_u.

Table 5: Plastic constitutive parameters of Ti6Al4V alloy made by EBM.

Bi-linear	Johnson-Cook		
E_t (MPa)	A (MPa)	B (MPa)	n
1952.8	786.54	60.63	0.50

3.6 Triaxiality and failure

The evolution of the overall load-displacement is shown in Figure 8. A good agreement between the experimental data and FE predictions can be observed for all the specimen configurations tested. In addition, a satisfactory agreement was obtained between the FE predictions and experimental measurements for the equivalent strain at the critical cross-section of the specimen, as shown in Figure 9. Figure 10 compares the strain fields given by the FE simulations and the DIC measurements at the onset of crack, again with reasonable correlation in terms of strain distributions.

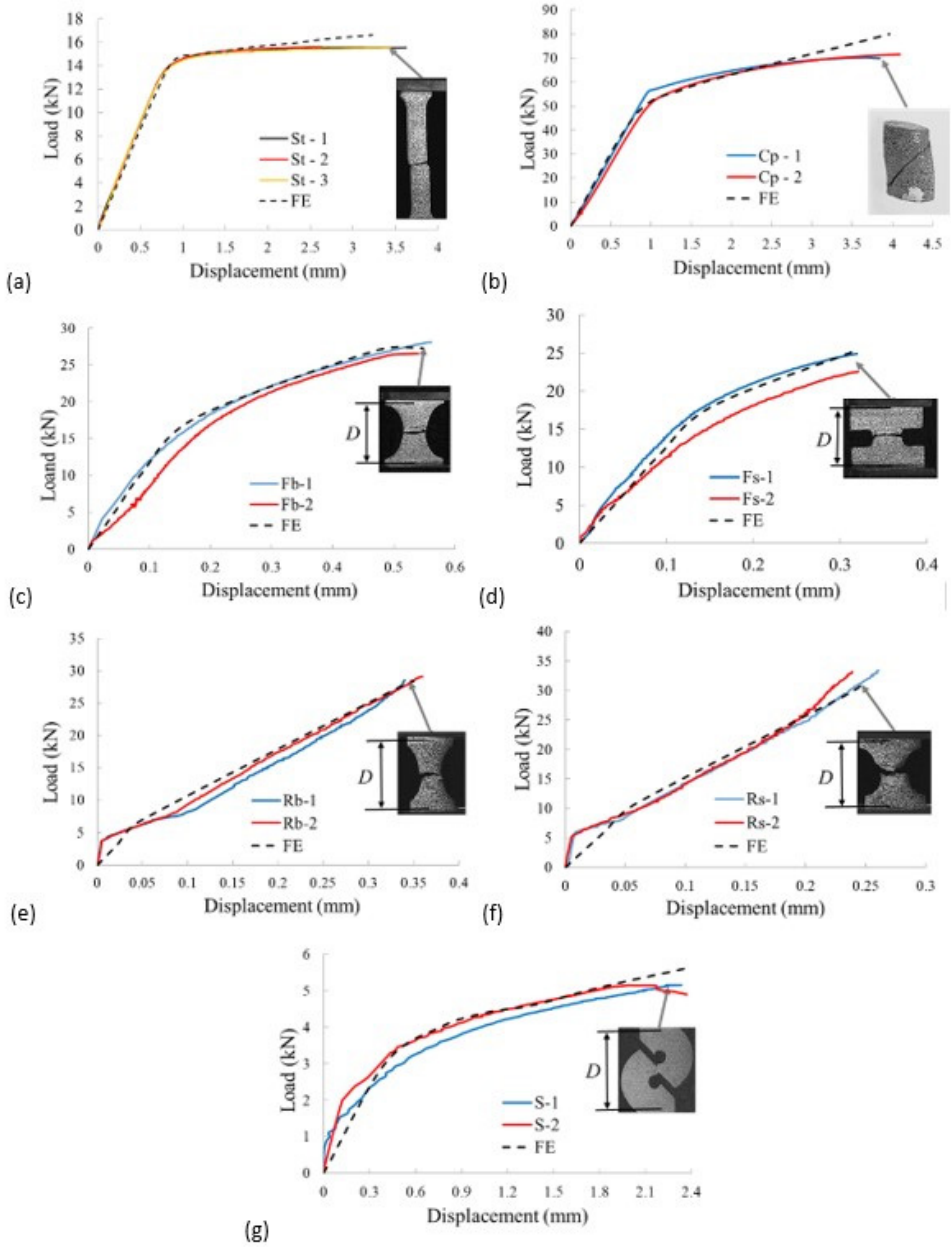

Figure 8: Experimental and numerical load-displacement responses of Ti6Al4V specimens made by EBM for (a) St, (b) Cp, (c) Fb (d) Fs, (e) Rb, (f) Rs and (g) S specimens.

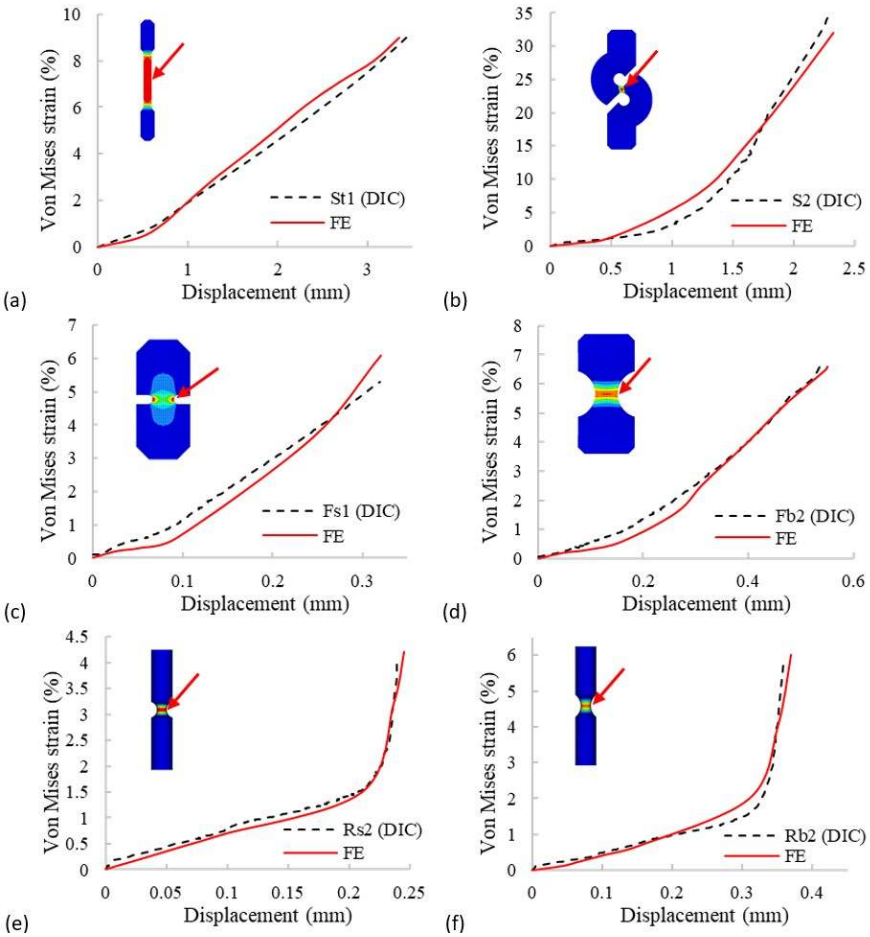

Figure 9: Experimental and numerical localized strain evolution at the critical cross-sections of specimens (a) St, (b) S (c) Fs, (d) Fb, (e) Rs and (f) Rb.

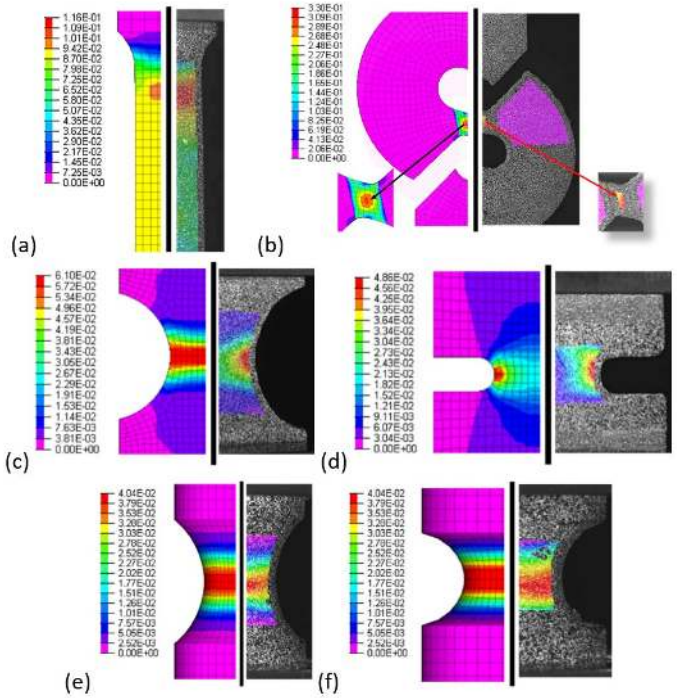

Figure 10: Comparison of the equivalent von Mises strains (mm/mm) between the FE simulations and experimental results: (a) St, (b) S (c) Fb, (d) Fs, (e) Rb and (f) Rs.

All the specimens failed in a brittle manner with minor necking. Tables 6-8 show the crack observed and its initiation position. Most cracks were initiated at an edge, likely due to relatively high surface roughness, then propagated through the cross-section. Once the crack initiated at the surface, it propagated through the specimen's cross-section. Brittle failure was also noted in the specimens Sd, Rb and Rs, which impresses once those specimens exhibited a ductile failure mode for the same alloy not made by AM [10, 12, 15]. The material's stress triaxiality and fracture strain were extracted from the FE simulation at the same ultimate displacement obtained at the onset of the failure of specimens, measured by the DIC. Then, the stress triaxiality and the related strain at the onset of failure were extracted from the same position at the critical cross-section where the crack initiation was observed. Table 9 summarises the fracture strains and stress triaxialities obtained by the current approach.

Table 6: The experimental crack initiation and the cross-section position considered for extracting the fracture strain and stress triaxiality on Cp, S and Sd samples.

Specimen ID	Experimental (: crack initiation)	FE Model (: position considered)	Stress Triaxiality
S-1			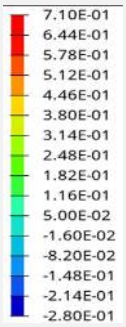
Sd-1			

Table 7: The experimental crack initiation and position considered for extracting the fracture strain and stress triaxiality on Fb and Fs samples.

Specimen ID	Experimental (: crack initiation)	FE Model (: position considered)	Stress Triaxiality
Fb-1		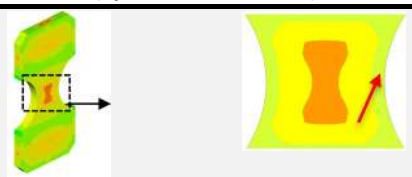	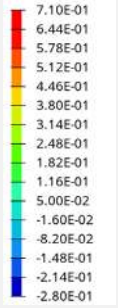
Fs-1		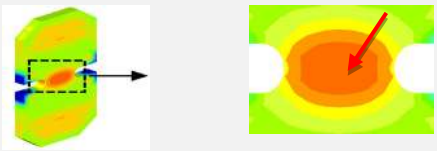	

Table 9 also presents the fracture strains obtained by DIC measurements for comparison purposes, with a reasonably good agreement between the both. It is worth pointing out that the DIC measurements provide the strain field near the edge and on the specimen surface. However, the critical strain extracted from the DIC correlates closely to the fracture strain predicted by the FE.

It is noted that stress triaxiality evolutes during the test, resulting in substantially different triaxiality levels from the initial predictions, as also reported in [10-13]. Thus, the stress triaxiality evolution is presented in Appendix 1 to support studies in this field in the future.

Table 8: The experimental crack initiation and the cross-section position considered for extracting the fracture strain and stress triaxiality on Rb and Rs samples.

Specimen ID	Experimental (: crack initiation)	FE Model (: position considered)	Stress Triaxiality
Rb-2		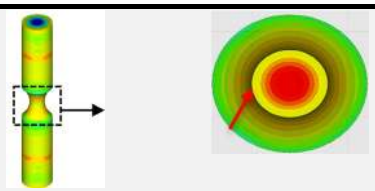	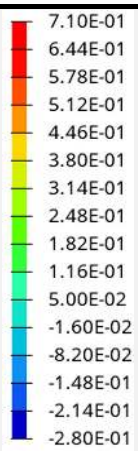
Rs-1		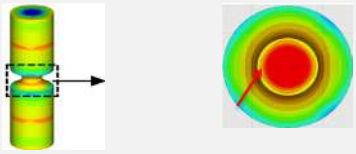	

Table 9: Summary of the stress triaxiality levels and ultimate strains obtained for the Ti6Al4V alloy made by EBM.

Specimen ID	Triaxiality, η	Fracture Strain, ε_f, from DIC (%)	Fracture Strain, ε_f, from FE (%)
C	-0.28	25.9 ± 0.1*	27.3
S	0.00	34.8 ± 4.2	30.0
St	0.33	8.9 ± 2.0	9.0
Fb	0.40	7.2 ± 0.6	6.6
Fs	0.52	4.8 ± 1.4	6.4
Rb	0.60	5.6 ± 0.5	6.0
Rs	0.71	4.6 ± 0.8	4.1

*Obtained from UTM crosshead displacement.

Table 9 is summarised in Figure 11, which highlights EBM Ti6Al4V has a strong dependence between stress triaxiality and fracture strain. In general, the material presents the influence of stress triaxiality similar to that expected for metallic alloys, with a low ε_u for higher η and a high ε_f at negative η. Bao and Wierzbicki [13] proposed an interpolation equation applicable to the low, medium and high triaxiality ranges as

$$\varepsilon_{u=}\begin{cases} 0.08(\eta+0.33)^{-0.40} & (\eta<0) \\ 0.44\eta^2-1.26\eta+0.46 & (0<\eta<0.4), \\ 0.07\eta^{-1}-0.06 & (\eta>0.4) \end{cases} \tag{7}$$

With those parameters being defined by an optimisation algorithm. Figure 11 also compares the response of the same alloy as-rolled and annealed [20, 33] with the behaviour obtained in this study related to EBM. It is evident that Ti6Al4V parts processed by EBM are different from those made by other manufacturing techniques, which indicates the need for a detailed fracture analysis for the EBM material.

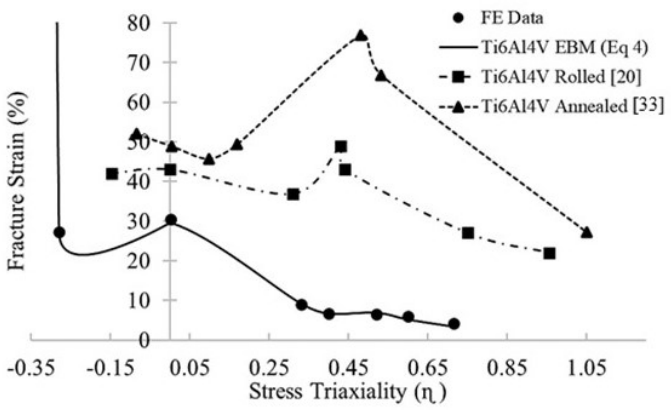

Figure 11: The relationships between stress triaxiality and fracture strain for the Ti6Al4V manufactured by EBM, Rolled and Annealed processes.

The Ti6Al4V alloy made by EBM presents a distinguished response at $\eta \sim 0$ and at $\eta > 0.3$. The alloy exhibits a relatively high ε_f at $\eta \sim 0$, where the failure is mainly governed by shear and void nucleation, which is usually relatively low compared to specimens produced by techniques other than AM in general or EBM. It suggests that the melted layer interfaces limit the voids and defects propagation between the melt pools and, as a result, enhance the ultimate strain, as presented in Figure 12(a). Thus, the material requires more energy for fracturing through the deposited layers.

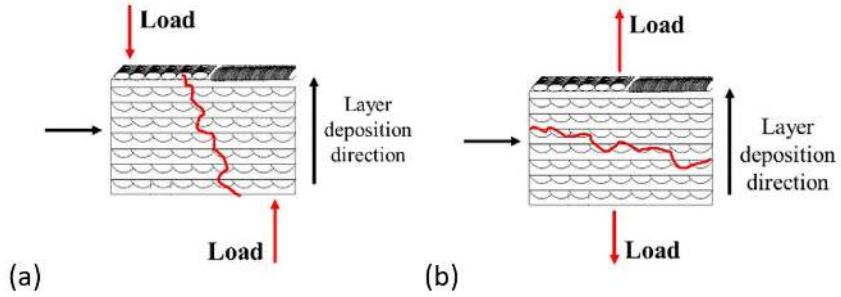

Figure 12: Fracture details of (a) S and (b) St specimens.

For the cases with $\eta > 0.3$, there is no evident influence of the triaxiality at the fracture strain, in which the specimens are governed by void nucleation and coalescence. In general, the non-AM alloys exhibit a strong influence of the stress triaxialities in this region, presenting a higher ε_f at $\eta \sim 0.3$, and then ε_f reduces as η increases. It was suggested that the layer interfaces (or melt pools) influence the Ti6Al4V response, triggering the material's fracture with a minor influence of the stress triaxiality and the loading is applied perpendicularly to the building direction, Figure 12(b),

3.7 Fracture modelling and evaluation

The damage parameters were obtained by curve fitting implemented as presented in Figure 13, with the related parameters being summarised in Table 10. Only positive stress triaxialities were considered in the interpolation due to limitations imposed by JC formulation for covering a wide range of stress triaxialities. As a result, an average deviation of less than 6.9% was reached. Additionally, the EPS failure criterion was defined for comparison purposes, extracted from the material's uniaxial tensile response obtained for specimen St, also presented in Figure 13 and Table 9.

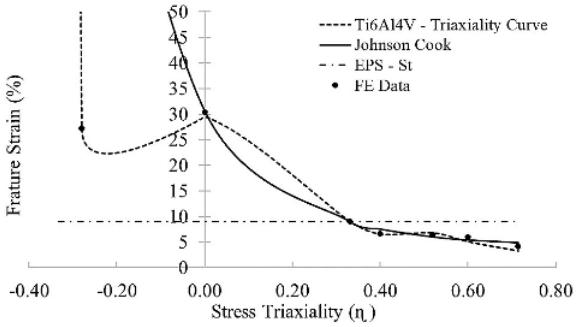

Figure 13: The Ti6Al4V made by EBM with failure prediction according to the JC damage model.

Table 10: Johnson Cook and EPS failure parameters for the Ti6Al4V made by EBM.

JC damage parameters			EPS
H_1	H_2	H_3	ε_f
0.03	0.326	-4.98	0.089

Figure 14(a) shows the experimental load-displacement response observed from the bifailure samples. The samples were loaded under tension, with the overall displacement being measured at the specimen's lower and bottom positions by DIC. The load initially increased, followed by a non-linear stage until a first drop due to the initial failures at positions 1 and 2 of the specimen. These failures occur almost simultaneously at a displacement between 0.2-0.4 mm and a high stress triaxiality (tension dominated). After this, the specimen was loaded continuously, with only position 3 remaining intact. It results in a second increase in the load observed beyond the 0.4 mm displacement. The material is loaded at a low stress triaxiality (shear dominated) until the failure at position 3. A good agreement was observed between the two samples tested, and Figure 14(b) shows the stress triaxiality evolution at positions 1-2 and 3.

The numerical prediction of the bifailure load-displacement response was initially obtained using the EPS failure criterion. The EPS failure criterion's limitations in predicting the alloy failure are evident in Figures 14(a) and 14(c). This approach considers the same strain-to-failure for any stress triaxiality state, which can be noted for the ultimate strain given for positions 1-2 and position 3 in Figure 14(c), different from that observed experimentally. This approach also overestimated the fracture loading for the failure at positions 1-2. Thus, using the EPS failure criterion is not suitable to provide reliable predictions of the response of the Ti6Al4V samples made by EBM.

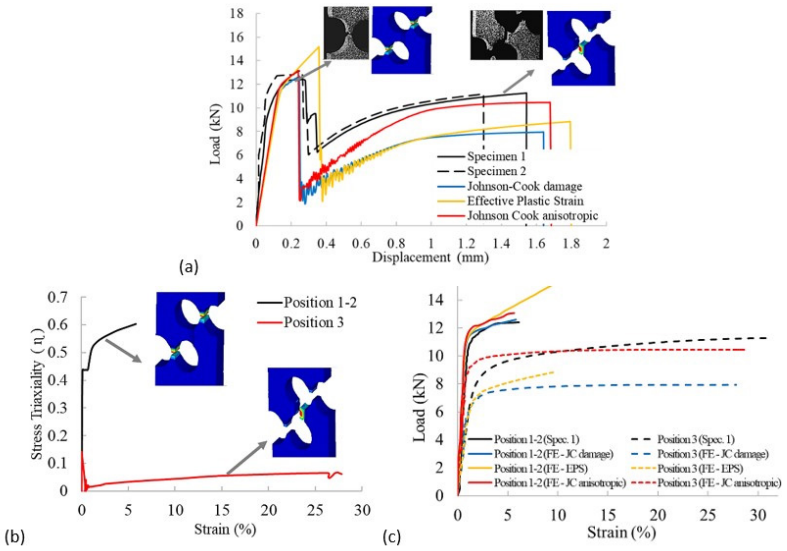

Figure 14: Triaxiality-based failure model evaluation: (a) numerical and experimental comparison of ad-hoc specimen load-displacement response, (b) stress triaxiality evolution in the ad-hoc specimen critical positions and (c) numerical and experimental comparison of the load-strain evolution in the ad-hoc specimen positions 1-2 and 3.

The FE prediction of the bifailure behaviour using JC damage was better when compared to EPS, once the JC provided a reasonable prediction for the failure strain at positions of 1-2 and 3. However, there was a discrepancy of about 29% between the loading predicted by FE and determined experimentally after failure at positions of 1-2. Figure 14(c) shows that the predicted ultimate strain levels at positions 1-2 and 3 are 0.058 and 0.278, respectively, which are close to 0.061 and 0.313 given by the experimental measurements. This discrepancy indicates that the limitation is not given by the relationship between triaxiality and the ultimate strain.

According to Zhai et al. [24], the Ti6Al4V samples made by EBM can exhibit anisotropic behaviour due to the microstructure resulting from the layer-by-layer nature of manufacturing. Therefore, an assessment was conducted by including anisotropic properties in the material's constitutive model, as presented in Appendix 2. As shown in Figures 14(a) and 14(c), the inclusion of anisotropic properties to the material modelling leads to a clear improvement in the bifailure prediction of the failure at position 3, with minor influence on the failure at positions 1-2. In this case, the difference between the loading prediction from FE and the experimental data at position 3 was reduced to 7.5%. Thus, the damage based on the stress triaxiality with regards to the anisotropic behaviour of the material provided a better prediction of the mechanical response of the EBM Ti6Al4V.

4 CONCLUSIONS

This paper has shown that the fracture mechanism of the Ti6Al4V parts produced by EBM additive manufacturing is dependent on stress triaxiality. Additionally, the relatively poor surface finish influences the mechanical behaviour, as evidenced by the cracks initiated at the surfaces of the specimen. The relationship between the fracture strain and stress triaxiality level was defined using combined experimental-numerical approaches.

The elastoplastic and damage parameters have been defined (Table 5 and Table 10), and explicit FE models have been developed to predict the mechanical behaviour of the samples investigated. The FE modelling provides reasonably good simulation results for specimens with different configurations when loaded at high strain levels and with various triaxialities.

Finally, the methodology used and the constitutive parameters obtained have been evaluated using an ad-hoc specimen. It has been demonstrated that the damage model based on stress triaxialities provided a better prediction of the response of EBM Ti6Al4V to high deformation levels and the onset of failure. The numerical predictions are significantly improved by taking the anisotropic behaviour of the alloy into account. Thus, the discrepancy between the simulated and experimental results is within a range from 4.9 to 7.5%, in terms of the stress triaxiality at three critical locations. In addition, based on the results, it is not recommended to use the effective plastic strain (EPS) failure criterion to make a reliable prediction of the mechanical response of the alloy.

The mechanical characterisation and modelling outputs of the EBM Ti6Al4V can be used for designing engineered components, able to predict the material behaviour to the ultimate condition and failure in a more accurate way. The use of FE modelling also reduces development time and cost in the industry.

ACKNOWLEDGMENTS

The authors acknowledge the Brazilian National Council for Scientific and Technological Development (CNPq) by grant number 436160/2018-8 and Dr. Nesma Aboulkair for supporting with insightful comments.

Author's Contributions: Conceptualisation, T Sartor, RC Santiago; Methodology, T Sartor, RC Santiago; Investigation, T Sartor; Writing - original draft, T Sartor, RC Santiago; Writing - review & editing, JV Lopes da Silva, G Zhongwei; Supervision, RC Santiago

Editor: Marco L. Bittencourt

REFERENCES

[1] ISO/ASTM 52900:2015(E). Standard Terminology for Additive Manufacturing – General Principles – Terminology, 2015.

[2] Volpato N, Silva JVL. Aplicação Direta da Manufatura Aditiva na Fabricação Final. In: Volpato N. Manufatura Aditiva, Tecnologias e Aplicações da Impressão 3D. 1st ed. São Paulo: Blucher; 2017. p.324-344.

[3] Tammas-Williams S, Zhao H, Léonard F, Derguti F. Todd I, Prangnell PB XCT analysis of the influence of melt strategies on defect population in Ti–6Al–4V components manufactured by selective electron beam melting. J. Materials Characterization. 2015; 102: 47-61.

[4] Rafi, HK, Karthik NV, Gong H, Starr TL, Stucker BE. Microstructures and mechanical properties of Ti6Al4V parts fabricated by selective laser melting and electron beam melting. J. Materials Engineering and Performance. 2013;22: 3872-3883.

[5] Longhitano GA, Larosa MA, Munhoz ALJ, Zavaglia CAC, Ierardi, MCF. Surface finishes for Ti-6Al-4V alloy produced by direct metal laser sintering. J. Materials Research. 2015; 18: 838-842.

[6] Fox JC, Moylan SP, Lane BM. Effect of process parameters on the surface roughness of overhanging structures in laser powder bed fusion additive manufacturing. In: Fox JC, Moylan SP, Lane BM. 3rd CIRP Conference on Surface Integrity. USA: CIRP CSI; 2016. 131-134.

[7] Hong M, Min BK, Kwon T. The influence of process parameters on the surface roughness of a 3D-printed Co–Cr dental alloy produced via selective laser melting. J. Applied Sciences. 2016; 6:401.

[8] Kirchner A, Kloden B, Luft J, Weibgarber T, Kieback B. Process window for electron beam melting of Ti-6Al-4V. J. Powder Metallurgy, 2015; 58: 246-249.

[9] Liu S, Shin YC. Additive manufacturing of Ti6Al4V alloy: A review. J. Material and Design. 2019; 164: 107-552.

[10] Driemeier L, Moura RT, Machado IF, Alves M. A Bifailure specimen for accessing failure criteria performance. Int. J. Plasticity. 2015; 72: 62-86.

[11] Bao Y. Dependence of ductile crack formation in tensile tests on stress triaxiality, stress and strain ratios. J. Engineering Fracture Mechanics. 2005; 72: 505-522.

[12] Wierzbicki T, Bao Y, Lee TW, Bai Y. Calibration and evaluation of seven fracture models. Int. J. Mechanical Science. 2005; 47: 719-743.

[13] Bao Y, Wierzbicki T. On the fracture locus in the equivalent strain and stress triaxiality space. Int. J. Mechanical Science. 2004; 46: 81-98.

[14] Wenchao L, Fangfang L, Tianhua Z, Harm A. Ductile fracture of Q460 steel: effects of stress triaxiality and lode angle. J. Constructional Steel Research. 2016; 123: 1-17.

[15] Calle M, Verleysen P, Alves M. Benchmark study of failure criteria for ship collision modelling using purpose-design tensile specimen geometries. Int. J. Marine Structures. 2017; 53: 68-85.

[16] Sjöberg, T., Kajberg, J., Oldenburg, M. Fracture behaviour of Alloy 718 at high strain rates, elevated temperatures, and various stress triaxialities. Engineering Fracture Mechanics, 2017; 178: 231-242

[17] Vigano F, Manes A, Giglio M. Calibration of fracture locus for the ti-6al-4v titanium alloy. In: Vigano F, Manes A, Giglio M. 18 European Conference on Fracture. Itally: ECF; 2010.

[18] Morales E, Yoneda A, Driemeier L, Celeghini R, Alves M. Numerical and experimental study of failure in steel beams under impact conditions. In Proceedings of the 10th World Congress on Computational Mechanics, Blucher Mechanical Engineering Proceedings, v. 1, n. 1. São Paulo: Blucher, 2014, DOI 10.5151/meceng-wccm2012-19366.

[19] Tang B, Wang Q, Guo N, Li X, Wang Q, Ghiotti A, Bruschi S, Luo Z. Modelling anisotropic ductile fracture Behaviour of Ti-6Al-4V titanium alloy for sheet forming applications at room temperature. International Journal of Solids and Structures. 2020; 207: 178-195.

[20] Hammer J, Seidt J, Gilat A. Influence of Stress State on the Ductile Fracture of Ti-6Al-4V, 2014. In: Jay C. (eds) Fracture and Fatigue, Volume 7. Conference Proceedings of the Society for Experimental Mechanics Series. Springer, Cham. https://doi.org/10.1007/978-3-319-00765-6_13.

[21] Mocko W, Kostrzewski C, Brodecki A. Influence of triaxiality on the fracture Behaviour of ti6al4v titanium alloy at impact loading conditions. In: Mocko W, Kostrzewski C, Brodecki A. 7 Conference on Mechanics and Materials in Design. Portugal: ICMMD; 2017.

[22] Wang, B., Xinran, X., Astakhov, V. P., Liu, Z. A quantitative analysis of the transition of fracture mechanisms of Ti6Al4V over a wide range of stress triaxiality and strain rate. Engineering Fracture Mechanics, 2020; 231:107020.

[23] Ziaja W., Finite element modelling of the fracture Behaviour of surface treated Ti-6Al-4V alloy. J. Computational Materials Science and Surface Engineering. 2009; 1: 53-60.

[24] Zhai Y, Galarraga H, Lados DA. Microstructure, static properties, and fatigue crack growth mechanisms in Ti-6Al-4V fabricated by additive manufacturing: LENS and EBM. J. Engineering Failure Analysis. 2016; 69: 3-14.

[25] Nalli F, Cortese L, Concli F. Ductile damage assessment of Ti6Al4V, 17-4PH and AlSi10Mg for additive manufacturing. Engineering Fracture Mechanics, 2021; 241: 107395.

[26] Nasrazadani, S., Hassani, S. Modern analytical techniques in failure analysis of aerospace, chemical, and oil and gas industries. In: Handbook of Materials Failure Analysis with Case Studies from the Oil and Gas Industry. Butterworth-Heinemann, 2016, Pages 39-54.

[27] ARCAM. Ti6Al4V Titanium Alloy. 2019. 3 p. Available in: <http://www.arcam.com/wp-content/uploads/Arcam-Ti6Al4V-Titanium-Alloy.pdf>. Accessed in: 17 mar. 2019.

[28] American Society for Testing and Materials. ASTM F2924-14. Standard specification for additive manufacturing titanium-6 aluminum-4 vanadium with powder bed fusion. EUA: ASTM; 2017.

[29] Anderson TL. Fracture Mechanics - Fundamentals and Applications. New York: CRC Press; 2005. 630p. ISBN: 978-1-4200-5821-5.

[30] Severino B, Couto A, Reis D. Aguiar C, Castagnet M, Neto C. Study of high temperature mechanical Behaviour of the thermally oxidised Ti-6Al-4V alloy. Materialwissenschaft und Werkstofftechnik, 2014, 45. 10.1002/mawe.201400226.

[31] American Society for Testing and Materials. ASTM A370-08ª. Standard Test Methods and Definitions for Mechanical Testing of Steel Products. EUA: ASTM; 2008.

[32] Hallquist J. LS-Dyna Theory Manual. United States; 2006.

[33] Giglio M, Manes A, Vigano F. Ductile fracture locus of Ti–6Al–4V titanium alloy. International Journal of Mechanical Sciences, 2012; 54: 121-135.

APPENDIX 1 – EVOLUTION OF THE STRESS TRIAXIALITY

Figure A1 summarises the evolution of stress triaxiality of each specimen configuration studied when loaded. As observed, the stress triaxiality varies during the loading of the specimens. It was also noted that samples with axisymmetric shapes presented higher changes in the triaxiality during the test.

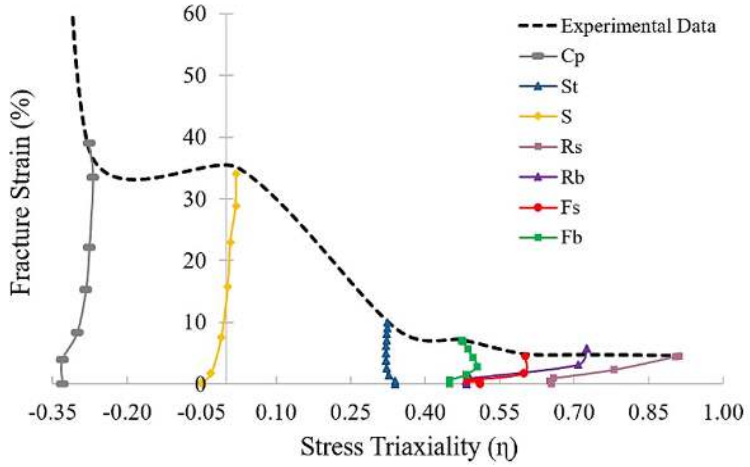

Figure A1. FE prediction of the evolution of stress triaxiality during loading.

APPENDIX 2 – ANISOTROPIC PARAMETERS OF BEM TI6AL4V

Elasto-plastic anisotropic parameters of the EBM Ti6Al4V were extracted from [4], summarised in Table 8. Those parameters were incorporated in the explicit FE models in addition to the stress triaxiality-based damage parameters obtained.

Table B1: Anisotropic elasto-plastic parameters used to model the Ti6Al4V made by EBM.

	E (GPa)	A (MPa)	B	n
X and Y directions	130.00	978.00	60.60	0.50
Z direction	94.30	786.54	60.60	0.50